MATERIALS CHEMISTRY FRONTIERS

RESEARCH ARTICLE

View Article Online
View Journal

Cite this: DOI: 10.1039/d5qm00390c

Double-layer absorbers based on $Co_{0.2}Ni_{0.4}Zn_{0.4}Fe_2O_4$ and $Ti_3C_2T_x$ composites for microwave absorption through optimal combination

Jianping Peng, †[a] Peijiang Liu,†*[b] Shanzheng Zhao,[a] Shiyu Zhang,[a] Liguo Xu,[e] Zibao Jiao*[c] and Zhenkai Huang*[d]

Double-layer absorbers serve the purpose of achieving high transmission efficiency and attenuation intensity in real-life applications. MXene-based composites exhibit huge potential in absorbing electromagnetic (EM) waves. In this work, $Co_{0.2}Ni_{0.4}Zn_{0.4}Fe_2O_4$ (CNZF) ferrites and $Ti_3C_2T_x$/$Co_{0.2}Ni_{0.4}Zn_{0.4}Fe_2O_4$ ($Ti_3C_2T_x$/CNZF) composites were fabricated *via* a hydrothermal method. XRD, FT-IR, XPS, SEM, and TEM were employed to analyze the composition and morphology of the samples. Specifically, microwave absorption properties of the single-layer and double-layer absorbers composed of CNZF and $Ti_3C_2T_x$/CNZF at varying thicknesses, were studied. For the double-layer absorber with CNZF as the matching layer (0.4 mm) and $Ti_3C_2T_x$/CNZF as the absorbing layer (2.4 mm), the maximum reflection loss (R_L) reached −44.4 dB at 7.6 GHz. This represented an exceptionally strong absorption performance at a relatively low frequency with a remarkably thin total absorber thickness of only 2.8 mm, overcoming the typical limitations of achieving high absorption at lower frequencies which often require thicker absorbers. The optimized double-layer structure demonstrates a practical solution for developing lightweight, thin, and high-performance microwave absorbers. The improved microwave absorption performance can be attributed to enhanced interfacial polarization, multiple reflections and scattering, as well as the rational layer configuration. These findings suggest that $Ti_3C_2T_x$/CNZF-based double-layer absorbers are promising candidates for achieving high-performance, thin microwave-absorbing materials.

Received 23rd May 2025,
Accepted 7th July 2025

DOI: 10.1039/d5qm00390c

rsc.li/frontiers-materials

1. Introduction

Currently, electromagnetic (EM) pollution and interference pose significant threats to information security, public health, the environment, and military operations, driven by the ubiquitous use of computers, Wi-Fi, remote sensors, fifth-generation mobile communications (5G), phones, and radars.[1–4] Various methods have been proposed to mitigate EM energy, and to date, the most effective approach for shielding against EM energy and reducing EM pollution is the use of EM absorbing materials. As functional materials, EM absorbers attenuate EM waves efficiently by transforming EM energy into heat or dissipating waves through interference.[5–8] Consequently, the development of ideal absorbing materials with light weight, broad absorption bandwidth, strong absorption, environmental adaptability, and thin profiles is attracting unprecedented attention.

Magnetic materials have historically played an important role in high-frequency microwave absorption.[9–11] However, they often fail to meet the requirements of thinness, lightness, strength, and broad bandwidth due to inherent limitations such as high density, weak mechanical properties, and limited absorption performance. Consequently, magnetic absorbers are typically employed as reinforcing components blended with other materials to synergistically attenuate EM waves.[12–14] For instance, researchers synthesized a 3D composite hydrogel of rGO/α-Fe_2O_3 *via* hydrothermal processing, achieving a maximum absorption of −33.5 dB at 7.12 GHz with a 5.0 mm coating thickness.[15] In contrast, 2D hierarchical composites

[a] School of Environment and Chemical Engineering, Foshan University, Foshan 528000, China
[b] Science and Technology on Reliability Physics and Application Technology of Electronic Component Laboratory, the Fifth Electronics Research Institute of the Ministry of Industry and Information Technology, Guangzhou 510610, China. E-mail: cz2343222@163.com
[c] Jiangsu Urban and Rural Construction Vocational College, ChangZhou 213147, P. R. China. E-mail: jiaozibao@126.com
[d] School of Materials and Energy, Foshan University, Foshan 528000, China. E-mail: hzk@fosu.edu.cn
[e] College of Light Chemical Industry and Materials Engineering, Shunde Polytechnic, Foshan 528333, China
† These authors contributed equally to this work.

have garnered significant attention in microwave absorption owing to their multi-scale architectures, which generate novel interface behaviors and host–guest synergistic effects.[16–19] This interfacial polarization in laminated structures dissipates EM energy through multiple pathways.

Recently, a novel class of 2D materials—transition metal carbides/nitrides (MXenes)—has emerged as promising absorbers because of their light weight and strong EM wave attenuation.[20–24] The layered structure of MXenes provides not only high specific surface area but also stable dielectric loss (5–13) from interfacial polarization. Crucially, HF etching functionalizes MXene surfaces with T_x groups (–O, –OH, –F), introducing chemically active sites that enhance defect polarization.[25] These surface terminations further impart hydrophilicity and solution processability.[26] These properties establish MXenes as ideal microwave-absorbing candidates. For example, rapidly annealed $Ti_3C_2T_x$ MXenes achieved a minimum reflection coefficient of −48.4 dB at 11.6 GHz (50 wt% in wax).[27] Nevertheless, pure MXene absorbers often exhibit excessive conductivity from metallic characteristics, causing incident wave reflection.[28] To address this, combining MXenes with magnetic components provides an effective strategy to reduce reflectivity. Such multi-phase composites enable tunable functionality through compositional control, particularly by balancing magnetic and dielectric properties for optimal impedance matching and enhanced microwave attenuation.

In this work, we prepared MXene-based composites to enhance microwave absorption performance by incorporating CNZF ferrites into the surfaces and interlayer spaces of $Ti_3C_2T_x$ MXene ($Ti_3C_2T_x$/CNZF). The selected $Ti_3C_2T_x$ particles—where T denotes O, OH, or F functional groups—serve as the MXene material due to their established synthesis protocols and superior absorption capabilities.[22] Subsequently, the EM parameters and microwave absorption performance of single- and double-layer absorbers based on CNZF and $Ti_3C_2T_x$/CNZF composites were systematically investigated. The microwave absorption performance primarily depends on impedance matching and EM attenuation capabilities, including conductive loss, magnetic loss, and relaxation loss.[29,30] Effective impedance matching allows sufficient wave penetration instead of surface reflection, while strong attenuation ensures efficient EM energy dissipation. However, single-layer absorbers often fail to simultaneously satisfy both requirements because high loss capabilities typically cause impedance mismatch. In contrast, double-layer absorbers demonstrate superior broadband microwave absorption potential, as optimal impedance matching and internal loss can be achieved through strategic combination of matching and absorbing layers. Having established this layer design principle, we evaluated the microwave absorption performance across various layer configurations and thoroughly analyzed the underlying mechanisms of double-layer absorbers.

2. Experimental section

2.1 Preparation of $Ti_3C_2T_x$ MXene

To synthesize $Ti_3C_2T_x$ MXene, Ti_3AlC_2 phase was chosen as precursor powders and treated with the well-known etching method.[30,31] Briefly, 50 wt% HF solution (analysis; Sinopharm Group Co. Ltd, China) was carefully added to a plastic container that involves 0.1 mol Ti_3AlC_2 particles (200 mesh; Forsman Scientific Company, China) with continuously stirring at 60 °C. After 48 h, a majority of Al atoms were removed from the Ti_3AlC_2 phase, and the black viscous liquid was centrifuged some times until the pH was neutral. Whereafter, the as-obtained $Ti_3C_2T_x$ were re-dispersed in an aqueous solution containing 5 wt% sodium hydroxide and keep ultrasonication for 2 h to get the final intercalated MXene powders.

2.2 Preparation of hierarchical $Ti_3C_2T_x$/CNZF composite

The detailed course for synthesizing $Ti_3C_2T_x$/CNZF composite is described in Fig. 1. Briefly, the as-obtained $Ti_3C_2T_x$ MXene was dispersed in D.I. water, and then treated with vigorous ultrasonication and stir for 1 h. During the period, specific nitrate

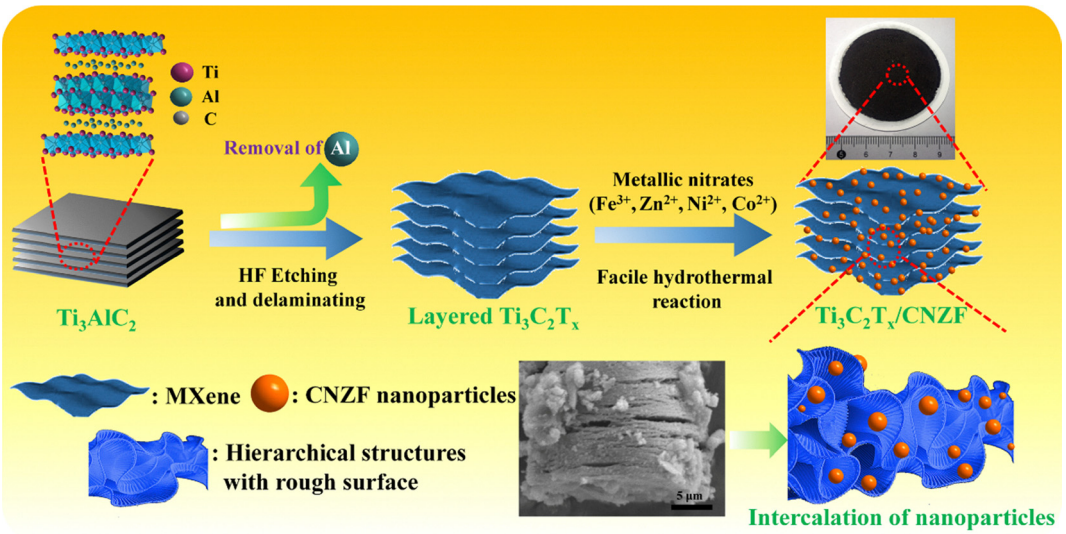

Fig. 1 Schematic illustration of the hydrothermal process for the $Ti_3C_2T_x$/CNZF composite.

precursors including cobalt nitrate hexahydrate $Co(NO_3)_2 \cdot 6H_2O$, nickel nitrate hexahydrate $Ni(NO_3)_2 \cdot 6H_2O$, zinc nitrate hexahydrate $Zn(NO_3)_2 \cdot 6H_2O$, and iron nitrate nonahydrate $Fe(NO_3)_3 \cdot 9H_2O$ (99% purity; Sinopharm Group Co. Ltd, China) were added into the above MXene dispersion and the pH value was fixed at 11 using ammonium hydroxide before sealing the autoclave. The molar ratio of metal cations $Co^{2+}:Ni^{2+}:Zn^{2+}:Fe^{3+}$ was fixed at 2.0 : 0.2 : 0.4 : 0.4 while the $Ti_3C_2T_x$ to CNZF mass ratio was precisely controlled at 1 : 2. The mixture was further stirred for another 0.5 h. After that, the viscous mixture was sealed in a Teflon-lined reactor and then underwent a hydrothermal course at 180 °C with a ramp rate of 5 °C min^{-1} using a programmable oven for 12 h. The resulting $Ti_3C_2T_x$/CNZF composites were filtered and washed employed degassed deionized water to prevent MXene oxidation. The resulting $Ti_3C_2T_x$/CNZF composites were filtered and dried at 60 °C in vacuum conditions for 10 h.

For EM parameter measurement, the samples were prepared by separately adding 60 wt% CNZF and $Ti_3C_2T_x$/CNZF in wax matrix. The homogeneous mixture was then subjected to a hot-pressing process at 65–70 °C to form dense and void-free ring-shaped specimens with 3.04 mm inner diameter and 7.00 mm outer diameter. This step is critical to ensure sample integrity for accurate electromagnetic parameter measurement by eliminating air pockets and achieving uniform dispersion of the absorptive fillers within the wax matrix. For convenience, the CNZF and $Ti_3C_2T_x$/CNZF represent the CNZF-wax and $Ti_3C_2T_x$/CNZF–wax composite.

2.3 Characterization

Morphologies of the samples were studied by using a transmission electron microscope (TEM, JEOL JEM2100) and field emission scanning electron microscope (FE-SEM, Zeiss Sigma, Germany), coupled with an energy dispersive spectroscopy (EDS). Structural analysis of the as-prepared samples was carried out by using X-ray powder diffraction (XRD, Bruker-D8, US) with Cu Kα radiation in the range of 5–80°. Chemical characterizations were examined by using Fourier transform infrared spectroscopy (FT-IR, Bruker Vector 33) and X-ray photoelectron spectroscopy (XPS, PHI 5300X). Static magnetic properties were recorded by using a vibrating sample magnetometer (VSM, Lakeshore, Model 7400 series). EM parameters of the specimens were recorded using a vector network analyzer (Agilent PNA N5224A, US) over 2–18 GHz by coaxial line method.

3. Result and discussion

The synthetic process of $Ti_3C_2T_x$/CNZF composite is elucidated in Fig. 1. Firstly, the MXenes were prepared by a well-known etching method using HF as the etching agent to remove Al layers. After obtaining the crude product, sodium hydroxide solution was used as an intercalating reagent to efficiently extend the distance of the interlayers by electronic attraction.[32] Secondly, by virtue of the enlarged interlamellar spacing, plenty of metal ions including Fe^{3+}, Ni^{2+}, Zn^{2+} and Co^{2+} can be bound on the surfaces of the $Ti_3C_2T_x$ particles and further grow into magnetic particles by a hydrothermal treatment. During this period, some TiO_2 nanoparticles have also formed from the abundant titanium source on the surfaces.[33,34] These anchored inorganic nanoparticles are supposed to serve as the blocker to keep the spacing expanding, which is good for multiple interfacial polarization.[35,36] The structures of the pure CNZF, $Ti_3C_2T_x$/CNZF, and oxidized $Ti_3C_2T_x$ were firstly characterized by using FTIR spectra in Fig. 2a. For pure CNZF nanoparticle, the hydroxyl groups are proved by broad O–H stretching vibration mode at 3000–3500 cm^{-1}, which indicates a hydrophilic ingredient on the surfaces of Fe_3O_4 nanoparticles. The exposed hydrophilic groups provide the possibility for intimately bonding with MXenes.[37] By reacting with CNZF nanoparticles, the bands over 400–700 cm^{-1} associated with the mixing metal–

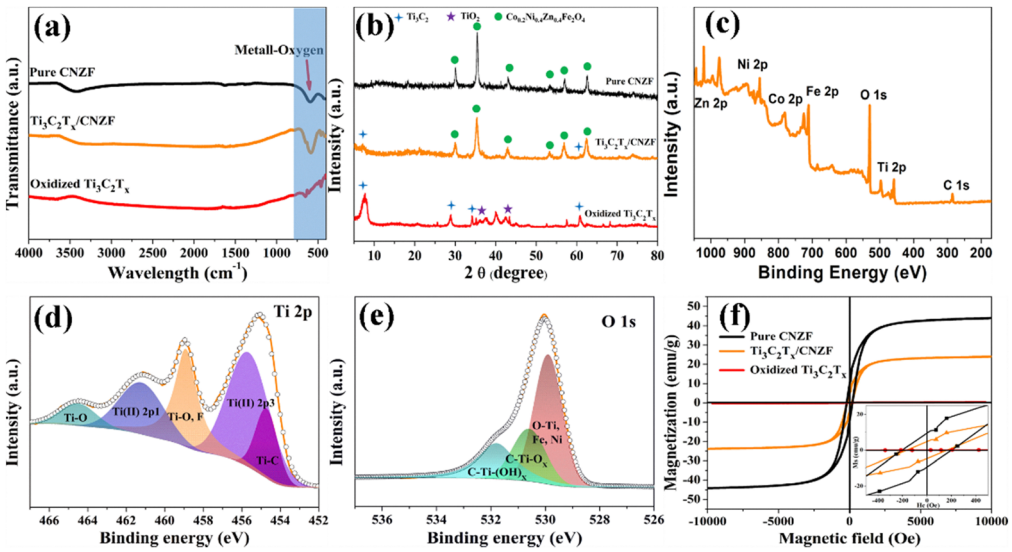

Fig. 2 Typical (a) FT-IR, (b) XRD, (c) XPS survey spectra, (d) Ti 2p spectra (e) O 1s spectra, and (f) magnetic hysteresis loops of the as-prepared samples.

oxygen stretching modes such as Ti–O, Zn–O, Ni–O, Co–O, and Fe–O are evident in curves.[38]

Fig. 2b shows the XRD patterns of the structures and phase composition for $Ti_3C_2T_x$/CNZF, pure CNZF, and oxidized $Ti_3C_2T_x$. Clearly, the pure CNZF shows a typical spinel structure with *Fd*3*m* space group, as is evidenced by the diffraction peaks located at 30.26°, 35.54°, 43.18°, 53.60°, 57.13°, and 62.69°, accordingly belonging to the (111), (220), (331), (400), (422), (511) and (440) planes to $Co_{0.2}Ni_{0.4}Zn_{0.4}Fe_2O_4$ ferrite (JCPDS Card No. 04-009-3215), respectively.[39] For $Ti_3C_2T_x$ MXene that suffering from the hydrothermal process, the Ti_3C_2 phases are in the majority, which coupled with the TiO_2 as the secondary phase. When CNZF nanoparticles were introduced into the MXenes, the crystal structures of spinel phases are retained, while there are two characteristic peaks of the Ti_3C_2 phases. Additionally, the intensities of the diffraction peaks are visibly weakened for both CNZF phase and Ti_3C_2 phase. On the basis of Debye–Scherrer equation, the calculated crystallite size of individual CNZF nanoparticle is about 15.1 nm, which is smaller than that of pure CNZF that calculated to be 23.2 nm. It is speculated that the $Ti_3C_2T_x$ effectively hinders the growth of the crystallite size for CNZF, as the magnetic nanoparticles may get stuck in the interlayers of the hierarchical structures. Another feature observed is that the (002) peaks of $Ti_3C_2T_x$/CNZF composites shift to a lower angle of ~7.20° compared with that of the oxidized $Ti_3C_2T_x$ (7.72°). This angular shift corresponds to an increase in interlayer spacing from approximately 11.4 Å to 12.3 Å according to Bragg's law calculations. The expansion originates from the successful intercalation of CNZF nanoparticles between the MXene layers during the hydrothermal process. These inserted particles physically separate the $Ti_3C_2T_x$ sheets while creating abundant heterogeneous interfaces. The enlarged interlayer distance directly facilitates enhanced interfacial polarization by providing greater space for charge accumulation at the MXene/CNZF boundaries. It should be noticed that the characteristic diffraction peaks of TiO_2 are not distinctly observable in the XRD pattern of $Ti_3C_2T_x$/CNZF composite due to the relatively low concentration of TiO_2 nanoparticles formed during partial oxidation compared to the dominant CNZF phase. Additionally, these TiO_2 particles likely exist in an amorphous or poorly crystalline state rather than a well-crystallized phase, further reducing their XRD visibility against the strong signals from the crystalline CNZF spinel structure and $Ti_3C_2T_x$ layers.

The successful synthesis of the $Ti_3C_2T_x$/CNZF composite is further proved by the XPS spectra. As seen in Fig. 2c, the surface elemental compositions of the $Ti_3C_2T_x$/CNZF composite are composed of Ti, C, O, Fe, Ni, Co and Zn with different ratios, while the Al peak completely disappear after etched, implying a great purity of $Ti_3C_2T_x$/CNZF composite.[40] The Ti 2p spectrum shows five deconvoluted peaks, corresponding to Ti–C ($2p_{3/2}$), Ti(II) ($2p_{3/2}$), Ti–O ($2p_{3/2}$), Ti(II) ($2p_{1/2}$), and Ti–O ($2p_{1/2}$) at around 454.7, 455.5, 458.5, 461.2 and 464.3 eV, respectively.[41] Simultaneously, the O 1s spectrum displays three deconvoluted peaks located at about 529.5, 530.4 and 531.7 eV, related to the O–Fe, Ni, Ti, C–Ti–O_x, and C–Ti–$(OH)_x$, respectively.[42] Obviously, the peak of O–Fe, Ni, Ti is higher than other peaks, indicating that the surfaces of the $Ti_3C_2T_x$ flakes are uniformly covered by the CNZF nanoparticles.[43] In addition, the Ti–OH bonds at 530.4 and 531.7 eV plainly indicate the presence of hydroxyl groups on the surface of Ti_3C_2. According to the previous research, the hydroxyl groups contribute to the formation of TiO_2 with higher intensity after suffering from the hydrothermal process.[44] In view of this situation, such contribution is further reinforced in our present work, for the hydroxyl groups serve as the active sites for ferrites to settle down and grow up, therefore inducing the heterogeneous interfaces. At some point, the CNZF ferrites not only give an enhancement to the multiple interfacial polymerization, but more strikingly they play a crucial role in balancing the interior dielectric and magnetic losses for impedance matching. In other words, the magnetic properties are also important for the intact absorbing material. Thus, we first studied the static magnetic properties of the as-obtained samples. As seen in Fig. 2f, both CNZF and $Ti_3C_2T_x$/CNZF composite present a S-type curve and are saturated in the magnetic field of 10 kOe, while the oxidized $Ti_3C_2T_x$ is undoubtedly non-magnetic. Due to the demagnetizing field caused by the oxidized MXene, the saturation magnetization (M_s) values and coercivity (H_c) for the $Ti_3C_2T_x$/CNZF composite decrease to 23.7 emu g^{-1} and 166.6 Oe, respectively. It is should be noticed that the M_s values are smaller than that of bulk $Co_{0.2}Ni_{0.4}Zn_{0.4}Fe_2O_4$ ferrite appeared in other work (M_s = 59.72 emu g^{-1}).[38] This feature can be explained that the magnetically inactive layers attach on the surfaces of CNZF nanoparticles, and this effect would become more serious as the particle size decreases, especially less than 20 nm.[45] In present work, although the M_s value for the $Ti_3C_2T_x$/CNZF composite is not superior, it has to point out that the magnetic loss, as well as the relevant impedance matching, should be reinforced to some extent, which will be described later.

The morphology of the samples is investigated by using SEM and TEM. As shown in Fig. 3a "accordion-like" structures of $Ti_3C_2T_x$ are well preserved after treated with sodium hydroxide. The TEM image exhibits the rough surfaces of the stacked multilayer structures (Fig. 3b). This roughness properly promotes the direct settlement of the inorganic particles on MXene surfaces by electrostatic interaction. In some special places, the detached layers are visibly curled up and combined with other layers to form cone shape, which also facilitates the decoration of the nanoparticles, and in turn further enhances the separation of the layers. After covered by ferrite nanoparticles, the $Ti_3C_2T_x$ surfaces get much rougher, reasonably ascribing to the emergence of the nanoparticles, as shown in Fig. 3c and d.[46] Nevertheless, the lamellate structures can be still observed in the $Ti_3C_2T_x$/CNZF composite and plenty of nanoparticles covering on the surface and intercalating into the hierarchical structures. Another feature observed from Fig. 3d is that the laminated structures not only emerge at the edge of MXene, but they also exist in the interior, as evidenced by the semitransparency in the composite. We may deduce that when the EM waves penetrate into the inner hierarchical structure, the incident waves are subjected to multiple reflection between nearby layers, thereby consuming more EM energies and

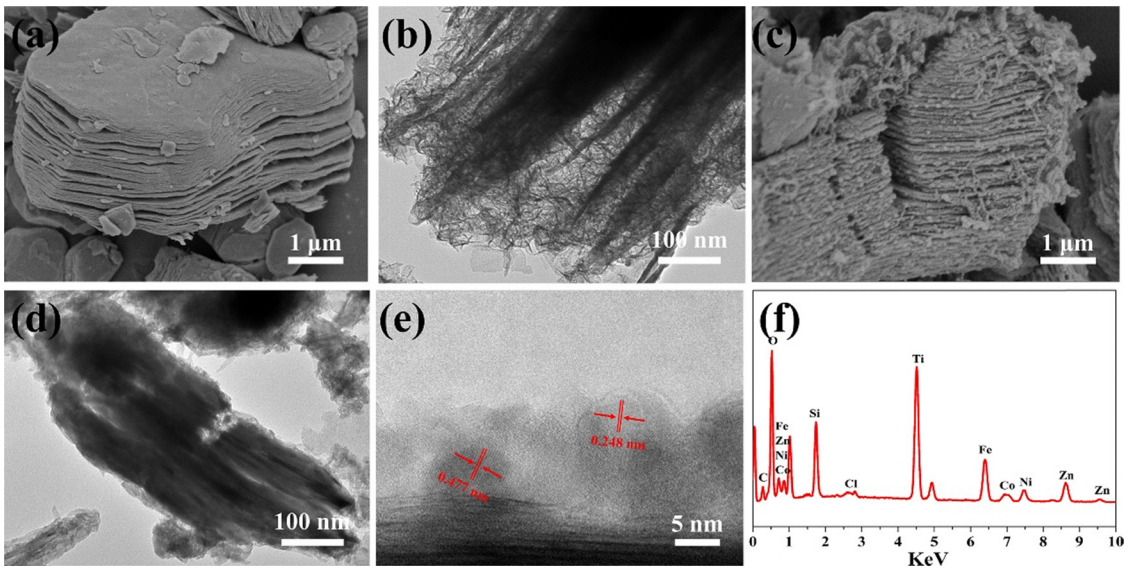

Fig. 3 Representative SEM images of (a) $Ti_3C_2T_x$ and (c) $Ti_3C_2T_x$/CNZF composite; TEM images of the lateral multilayered structures of (b) $Ti_3C_2T_x$ and (d) $Ti_3C_2T_x$/CNZF composite; (e) HR-TEM image and (f) EDS curve of the $Ti_3C_2T_x$/CNZF composite.

transforming into heat. In Fig. 3e, the HR-TEM image shows the lattice outlines of the newly prepared CNZF ferrites with sizes of 10–16 nm. The lattice spacings of the surface-concentrated particles are calculated to be around 0.248 and 0.477 nm, belonging to the (311) and (111) planes of spinel CNZF ferrite (JCPDS card no. 04-009-3215), respectively.[47] The elemental composition of $Ti_3C_2T_x$/CNZF was analyzed from EDS spectrum, which confirms the probable presence of component elements.

To illustrate the possible absorbing mechanisms, the related EM parameters are exhibited in Fig. 4. Conceptually, for EM parameters, the real parts including ε' and μ' refer to storage performance, and the imaginary parts including ε'' and μ'' mean energy dissipation.[43,48] For pure ferrite, both ε' and ε'' values (ε' = 3.9 and ε'' = 0.1) are predictably the smallest in all samples and keep constant with the frequency increasing. After reacted with MXene particles, ε_r for the $Ti_3C_2T_x$/CNZF composite significantly increases and begins to fluctuate across the whole frequency range due to the dipole polarization, which can not catch up with the pace of electric field change in gigahertz region.[49–52] The improved dielectric property of

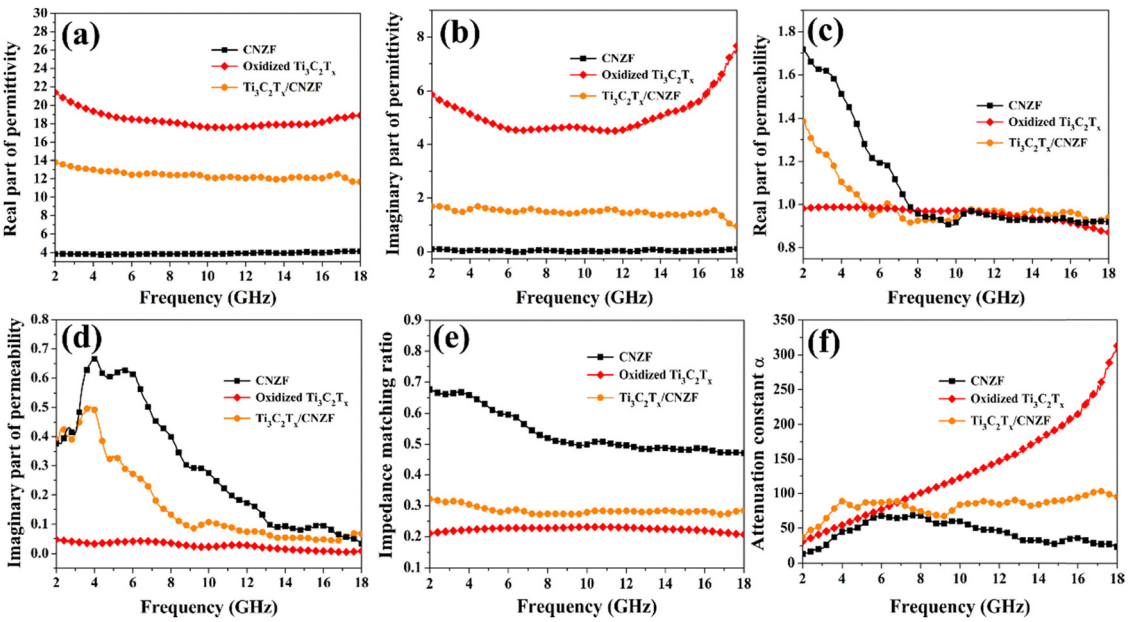

Fig. 4 Representative (a) and (c) real and (b) and (d) imaginary parts of the electromagnetic parameters; curves of (a) impedance matching ratio and (b) attenuation constant α of CNZF, oxidized $Ti_3C_2T_x$, and $Ti_3C_2T_x$/CNZF composite. (e) The impedance matching ratios and (f) the attenuation constant α of the as-prepared samples.

$Ti_3C_2T_x$/CNZF primarily attributes to the integrated polarization causing by its flake-like, laminated, and heterogeneous architectures. Based on 1/4 cancellation equation, great ε'' values are conducive to thin absorber thickness:[53,54]

$$d = n\lambda/4 = nc/4f_m\sqrt{\varepsilon_r\mu_r} \quad (1)$$

where λ, d, and f_m are the EM wavelength, absorber thickness, and absorbing peak frequency, respectively. Considering the EM data could be modulated by reasonably designing absorbers, such a result is critical for the arrangement of absorbing layers with proper ε_r values. Fig. 4c and d exhibit the μ_r plots of the as-synthesized samples. Pristine CNZF ferrite displays the largest value of all samples. After reacted with MXene, little changes have happened, where the μ' values firstly decrease from 1.4 to 0.9 over 2–10 GHz and then keep fluctuating in a gentle way at the rest of the frequency. By virtue of the high starting μ' values of $Ti_3C_2T_x$/CNZF, a promising impedance matching characteristic for the composite can be predicted. As for μ'', the $Ti_3C_2T_x$/CNZF composite reveals a strong multiple resonance peak at around 2–7 GHz owing to the natural resonance of ferrites, which arguably inherit the magnetic characteristics from the magnetic CNZF nanoparticles.[55–57] Unfortunately, like all other ferrites, the magnetic loss for the $Ti_3C_2T_x$/CNZF composite also exhibits a downward trend from 0.5 to nearly 0 as the frequency increases because of the Snoek's limitation.[18,58]

Overall, the exceptional microwave absorption capabilities originate from strategically engineered microstructural features. The expanded interlayer spacing of $Ti_3C_2T_x$ observed in Fig. 1 facilitates enhanced interfacial polarization by accommodating larger dipole moments under alternating electromagnetic fields. Concurrently the controlled CNZF particle size distribution centered at 10–16 nm in Fig. 3e optimizes magnetic resonance effects by maintaining single-domain characteristics while providing sufficient surface area for multi-interfacial polarization. Critically the intimate contact at $Ti_3C_2T_x$/CNZF interfaces creates localized charge accumulation zones that amplify conduction losses through electron hopping along MXene layers. This structural synergy generates complementary loss mechanisms where $Ti_3C_2T_x$ layered architecture dominates dielectric dissipation while CNZF nanoscale crystallites govern magnetic losses. Furthermore the heterointerface defects act as polarization centers that broaden the effective absorption bandwidth through additional relaxation processes.[59]

Taking into account these EM parameters, we can deduce that the CNZF nanoparticle has a finer impedance matching performance as the μ_r and ε_r for pure CNZF nanoparticle are pretty close. For the best-in-class absorber, the absorption properties are majorly determined by the impedance matching and EM attenuation.[49,60] At the first stage, well-matched impedance enables enough microwaves to transfer into the absorbers rather than be reflected on the surface, which is vital for further EM dissipation. Accordingly, we have compared the impedance matching ratios for all samples in Fig. 4e. Thanks to smaller dielectric properties, it is not surprising that the bare CNZF obtains the highest matching ratios of larger than 0.4 in the whole measurement frequency range compared with those of other samples. This means that optimal electromagnetic wave entry into the absorber with minimal reflection at the air–absorber interface. This contrasts with $Ti_3C_2T_x$/CNZF lower coefficient of less than 0.4 where impedance discontinuity causes significant wave reflection. The quantitative analysis confirms that positioning CNZF as the matching layer and $Ti_3C_2T_x$/CNZF as the loss layer maximizes synergistic effects.

Beyond ultra-wideband absorption performance, reliable dielectric stability under thermal stress represents a critical requirement for practical microwave absorbers. Fig. 5 shows the temperature-dependent complex permittivity of $Ti_3C_2T_x$/CNZF composites from 25 °C to 200 °C. As the temperature increases, both real and imaginary permittivity curves keep similar shapes but shift upward overall. This overall increasing trend demonstrates particularly pronounced sensitivity at lower frequencies. These dielectric variations are explained through Debye relaxation theory.[61] Temperature changes primarily affect polarization relaxation times. According to this theory, rising temperatures increase the thermal kinetic energy of activated molecules, accelerating the approach to steady-state conditions and consequently shortening relaxation time (τ). This mechanism directly enhances dielectric properties at elevated temperatures. Additionally, elevated temperatures significantly promote free electron and electron hole mobility within the aerogel structure, which increases electrical conductivity and thereby contributes substantially to dielectric loss enhancement.[62]

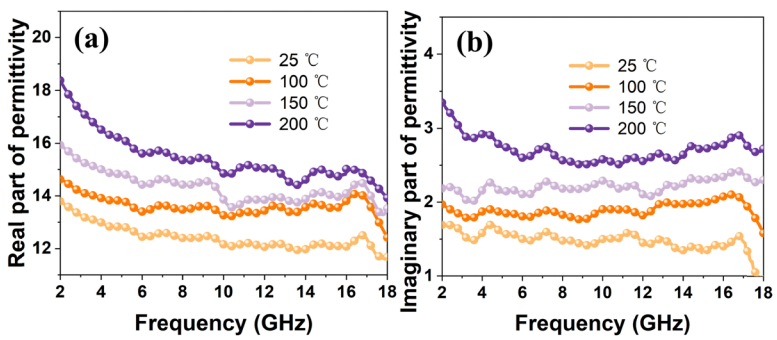

Fig. 5 Frequency dependences of (a) real and (b) imaginary parts of complex permittivity from 25 °C to 200 °C.

Besides the surficial matching characteristic, the inner microwave attenuation capability for a promising absorber is another considerable feature to determine the absorbing effectiveness, and could be expressed by the attenuation constant α:[63,64]

$$\alpha = \frac{\sqrt{2}\pi f}{c} \times \sqrt{(\mu''\varepsilon'' - \mu'\varepsilon') + \sqrt{(\mu''\varepsilon'' - \mu'\varepsilon')^2 + (\mu'\varepsilon'' + \mu''\varepsilon')^2}} \quad (2)$$

here f and c are the EM frequency and light velocity in free space, respectively. Fig. 4f presents the attenuation constant α of the as-prepared samples. As can be observed, the oxidized MXene possesses the relative higher attenuation values in the frequency range of 7–18 GHz, which is relying on the large dielectric loss capability. Comparatively, a weak attenuation constant α is distinguished for the bare CNZF. Although the attenuation capabilities of $Ti_3C_2T_x$/CNZF is not as high as those of the oxidized MXene in the relatively high frequency region, the composite illustrates a higher attenuation constant α at the frequency range of 2–7 GHz, in which the searching for ideal absorbers is still a great challenge. Accordingly, considering the combination effect of the low-frequency attenuation level as well as the moderate exterior matching character, the $Ti_3C_2T_x$/CNZF composite was reasonably selected as the absorbing layer.

Before we investigate the microwave absorption properties of the double-layer absorbing materials, the absorption performance of the single-layer absorbing materials have been analyzed for comparison purposes, and can be normally expressed by reflection loss (R_L) as following equation:[65]

$$R_L\ (\text{dB}) = 20\log|(Z_{in} - Z_0)(Z_{in} + Z_0)| \quad (3)$$

$$Z_{in} = Z_0\sqrt{\mu_r/\varepsilon_r}\tanh\left[j(2\pi fd/c)\sqrt{\mu_r\varepsilon_r}\right] \quad (4)$$

here Z_{in}, ε_r, μ_r and d is the normalized input impedance (377 Ω), complex permittivity, complex permeability and thickness of absorbers, respectively. Conceptually, the R_L value being less than −10 dB is equivalent to the absorption of 90% EM energies and regarded as the guidance for optimizing high-performance microwave absorbers. Fig. 6a–c show the theoretical R_L of single-layer absorbers based on pure CNZF, oxidized $Ti_3C_2T_x$ and $Ti_3C_2T_x$/CNZF composite over 2–18 GHz as the thicknesses increase from 1.0 to 5.0 mm. Obviously, the pure CNZF ferrite and oxidized $Ti_3C_2T_x$ have inferior absorbing effectiveness, *i.e.*, absorbing intensity and effective frequency bandwidth. Comparatively, the $Ti_3C_2T_x$/CNZF composite presents relatively optimized absorption properties with a maximum R_L value of −32.3 dB at 6.0 GHz and effective absorbing bandwidth of 1.8 GHz when the thickness reaches 3.5 mm. Whereas, the absorption performance for $Ti_3C_2T_x$/CNZF composite is not outstanding and can not achieve the quality for advanced absorbing materials in real-life application. This motivates us to pursue new kinds of absorbers based on $Ti_3C_2T_x$/CNZF composite.

In view of that, we have designed double-layer absorbers by virtue of wide effective bandwidth and reduced thickness for these kinds of materials. The following equation is used to calculate Z_{in} of double-layer absorbers, which is further plugged into the eqn (3) to acquire the R_L values.

$$Z_{in} = \frac{\sqrt{\frac{\mu_2}{\varepsilon_2}}\left(\sqrt{\frac{\mu_1}{\varepsilon_1}}\tanh\left[j\left(\frac{2\pi fd_1}{c}\right)\sqrt{\mu_1\varepsilon_1}\right] + \sqrt{\frac{\mu_2}{\varepsilon_2}}\tanh\left[j\left(\frac{2\pi fd_2}{c}\right)\sqrt{\mu_2\varepsilon_2}\right]\right)}{\sqrt{\frac{\mu_2}{\varepsilon_2}} + \sqrt{\frac{\mu_1}{\varepsilon_1}}\tanh\left[j\left(\frac{2\pi fd_1}{c}\right)\sqrt{\mu_1\varepsilon_1}\right]\tanh\left[j\left(\frac{2\pi fd_2}{c}\right)\sqrt{\mu_2\varepsilon_2}\right]} \quad (5)$$

where d_1 and d_2 are the thicknesses for layer 1 and 2, respectively.

As depicted in Fig. 7a, layer 1 and 2 represent the absorbing layer and matching layer, respectively. ε_1, μ_1, ε_2, and μ_2 are the EM parameters of the absorbing layer and matching layer, respectively. Taking into account the efficient penetration of microwaves on absorber surface, pure CNZF with a remarkable impedance matching ratio was selected as the matching layer. Fig. 7b shows the R_L of double-layer absorbing materials composed of the absorbing layer filled with $Ti_3C_2T_x$/CNZF composite and matching layer filled with CNZF ferrite with a fixed thickness of 2.7 mm. With the absorbing layer of 2.6 mm and matching layer of 0.1 mm, the double-layer absorber exhibits a maximum R_L of −42.7 dB at 7.7 GHz as well as an effective absorbing bandwidth of 2.3 GHz. Comparatively, the absorber, composed of a single absorbing layer with the same total thickness (2.7 mm), only achieves an inferior absorption property with the maximum R_L of −35.3 dB. Meanwhile, the effective absorbing bandwidth is also narrower than that of the above double-layer absorber. We believe that the improved microwave attenuation capability for double-layer absorbers is attributed to the well coupled assembly between the matching and absorbing layers. Therefore, the strategy by constructing double-layer absorbers is a feasible approach to achieve ideal

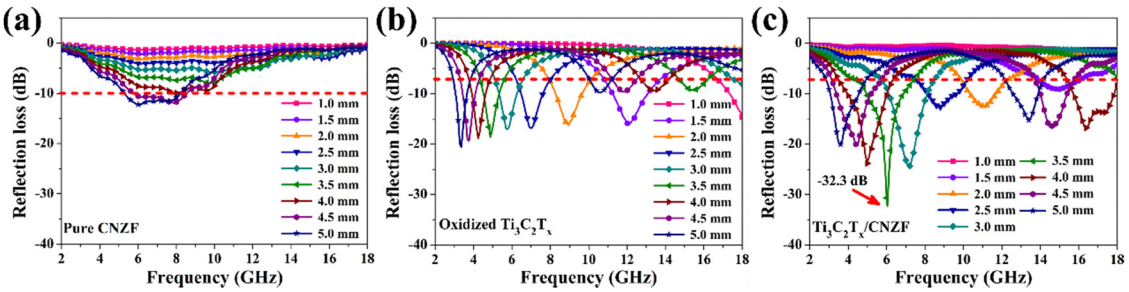

Fig. 6 Calculated R_L values of the single-layer absorbers for (a) CNZF, (b) oxidized $Ti_3C_2T_x$, and (c) $Ti_3C_2T_x$/CNZF composite over 2–18 GHz.

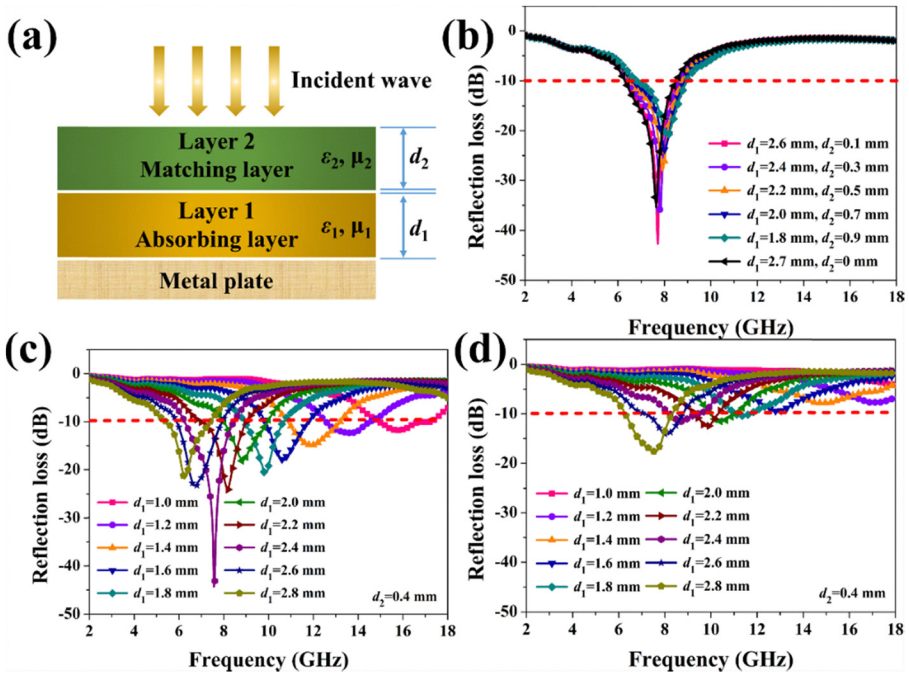

Fig. 7 (a) Typical schematic of double-layer absorbers; (b) calculated R_L values of the double-layer absorbers consisting of matching layer (CNZF) and absorbing layer ($Ti_3C_2T_x$/CNZF) with constant total thickness of 2.7 mm over 2–18 GHz; (c) R_L values of the double-layer absorbers consisting of matching layer (CNZF) with the fixed thickness of 0.4 mm and absorbing layer ($Ti_3C_2T_x$/CNZF) with varied thicknesses of 1.0–2.8 mm; (d) R_L values of the double-layer absorbers consisting of matching layer ($Ti_3C_2T_x$/CNZF) with the fixed thickness of 0.4 mm and absorbing layer (CNZF) with varied thicknesses of 1.0–2.8 mm.

EM wave absorbing materials. For further research in the microwave absorption performance of double-layer absorbers, the R_L values of the absorbers consisted of CNZF as the matching layer with a constant thickness of 0.4 mm and $Ti_3C_2T_x$/CNZF composite as the absorbing layer with varied thicknesses are illustrated in Fig. 7c. When the optimized thickness of absorbing layer is 2.4 mm, R_L reaches the maximum value of −44.4 dB at 7.6 GHz, coupled with an efficient bandwidth of 2.3 GHz. It is notable to address that R_L values realize a continuous frequency range from 5.4 to 17.2 GHz as the absorbing thicknesses increase from 1.0 to 2.8 mm. This finding provides the accessibility to adjust the absorbing frequency range through tuning the layer thickness. For comparison, the microwave absorption properties of the absorbers based on the matching layer of the $Ti_3C_2T_x$/CNZF composite and absorbing layer of CNZF have also studied in Fig. 7d. As the matching layer is fixed to 0.4 mm and absorbing layer increase from 1.0 to 2.8 mm, all the absorbers show poor attenuation capability including absorbing intensity and efficient bandwidth. The typical microwave absorption performance of double-layer absorbers with varied thicknesses is listed in Table 1. Obviously, the double-layer absorbers consisting of the $Ti_3C_2T_x$/CNZF as the absorbing layer and CNZF as the matching layer possess superior microwave absorption properties than the single-layer absorbers (CNZF or $Ti_3C_2T_x$/CNZF) or the double-layer absorbers based on CNZF as the absorbing layer and $Ti_3C_2T_x$/CNZF as the matching layer.

Table 1 Representative of the double-layer absorbers based on $Ti_3C_2T_x$/CNZF composite and their microwave absorption performance

Samples	Materials	Thickness (mm)	Total thickness (mm)	Maximum R_L (dB)	Peak frequency (GHz)	Bandwidth R_L < −10 dB (GHz)
1	Layer 1: $Ti_3C_2T_x$/CNZF	1.4	1.7	−15.9	12.7	2.3
	Layer 2: CNZF	0.3				
2	Layer 1: $Ti_3C_2T_x$/CNZF	1.9	2.0	−21.9	10.0	1.9
	Layer 2: CNZF	0.1				
3	Layer 1: $Ti_3C_2T_x$/CNZF	2.5	2.7	−46.4	7.8	2.3
	Layer 2: CNZF	0.2				
4	Layer 1: $Ti_3C_2T_x$/CNZF	2.6	2.7	−42.7	7.7	2.3
	Layer 2: CNZF	0.1				
5	Layer 1: $Ti_3C_2T_x$/CNZF	2.4	2.8	−44.4	7.6	2.3
	Layer 2: CNZF	0.4				
6	Layer 1: Fe_3O_4	3.2	3.7	−20.1	7.6	3.7
	Layer 2: MXene/Fe_3O_4	0.5				
7	Layer 1: Fe_3O_4	3.2	3.9	−26.2	6.5	3.6
	Layer 2: MXene/Fe_3O_4	0.7				

Table 2 R_L and effective bandwidth of some double-layer absorbers reported in recent years

Materials (layer 1: absorbing layer; layer 2: matching layer)	Thickness (mm)	Total thickness (mm)	Maximum R_L (dB)	Peak frequency (GHz)	Bandwidth $R_L < -10$ dB (GHz)	Ref.
Layer 1: cabbage-like $CoFe_2O_4$	1.0	2.6	−17.5	9.75	4.2	66
Layer 2: polypyrrole	1.3					
Layer 1: carbon nanofibers	1.03	3.01	−63.7	10.0	—	67
Layer 2: $Ba_2Co_2Fe_{12}O_{22}$@C core–shell nanofibers	1.98					
Layer 1: MWCNTs/$La_{0.6}Sr_{0.4}Mn_{0.5}Fe_{0.5}O_4$	1.0	2.0	−36.0	8.5	2.0	68
Layer 2: MWCNTs/$La_{0.6}Sr_{0.4}Mn_{0.5}Fe_{0.5}O_4$ coated with PEDOT	1.0					
Layer 1: MWCNTs/$BaTiO_3$/pitted carbonyl iron	1.5	3.0	−13.0	9.7	0.4	69
Layer 2: MWCNTs/$BaTiO_3$/pitted carbonyl iron	1.5					
Layer 1: FeSiAl/PLA	3.2	6.0	−45.6	14.88	3.92	70
Layer 2: FeSiAl–MoS_2–graphene/PLA	2.8					
Layer 1: MWCNTs/FeCoNi@C	0.5	2.5	−14	9.8	0.4	71
Layer 2: FeCoNi@C	2.0					
Layer 1: perpendicular $Ti_3C_2T_x$ MXene	—	3.3	−47.2	8.03	4.1	72
Layer 1: parallel $Ti_3C_2T_x$ MXene						
Layer 1: $Ti_3C_2T_x$/CNZF	1.4	1.7	−15.9	12.7	2.3	This work
Layer 2: CNZF	0.3					
Layer 1: $Ti_3C_2T_x$/CNZF	2.4	2.8	−44.4	7.6	2.3	This work
Layer 2: CNZF	0.4					

As exhibited in Table 2, the R_L values and effective bandwidth of the double-layer absorbers in this work are compared with existing bilayer designs from literature. The proposed double-layer architecture demonstrates great performance over comparative systems. This enhancement originates from optimized impedance matching dynamics and elevated attenuation constants-two decisive factors governing microwave absorption capabilities.

Based on the above results, three primary mechanisms contribute to the enhanced attenuation performance. First, as discussed, abundant CNZF nanoparticles formed on the surfaces and interlayers of layered MXene structures, generating $Ti_3C_2T_x$–CNZF, TiO_2–$Ti_3C_2T_x$, and TiO_2–CNZF interfaces and triple junctions. These interfaces accumulate bound charges, enhancing interfacial polarization and associated relaxation. Second, the multi-scale interfaces and architectures induce multiple reflections and scattering of EM waves, leading to significant energy dissipation through destructive interference. Third, optimal configuration of the matching layer (CNZF) and absorbing layer ($Ti_3C_2T_x$/CNZF) is critical for achieving superior microwave absorption. Specifically, CNZF provides exceptional impedance matching, while $Ti_3C_2T_x$/CNZF delivers strong attenuation. This strategically layered structure significantly enhances the absorption properties.

4. Conclusion

In summary, CNZF nanoparticles and $Ti_3C_2T_x$/CNZF composites were synthesized *via* hydrothermal processing. The composition and morphology were characterized by XRD, FT-IR, XPS, SEM, and TEM. The microwave absorption performance of single- and double-layer absorbers with varying thicknesses —composed of CNZF and $Ti_3C_2T_x$/CNZF—was systematically investigated. Owing to the strong EM attenuation capability of the $Ti_3C_2T_x$/CNZF layer and superior impedance matching of the CNZF layer, the double-layer structure exhibited promising performance. A maximum reflection loss (R_L) of −44.4 dB at 7.6 GHz was achieved with a 2.4 mm absorbing layer and 0.4 mm matching layer. This enhancement primarily resulted from improved interfacial polarization, multiple reflections/scattering, and optimized bilayer configuration. These findings demonstrate that such double-layer absorbers are a viable strategy for developing high-performance, low-profile microwave absorbers.

Author contributions

P. L. and Z. J. supervised and guided the project. P. L. designed the research. J. P. completed the fabrication process. J. P., Y. S., S. Z. conducted the measurement and analyzed the results. J. P. drafted the manuscript, and all authors contributed to the manuscript revision. All authors have given approval to the final version of the manuscript.

Conflicts of interest

The authors declare no competing interests.

Data availability

The data are available from the corresponding author on reasonable request.

Acknowledgements

This work was financially supported by the National Natural Science Foundation of China (22401045, 22301037), Natural Science Foundation of Guangdong Province (2022A1515110867), the National Key Research and Development Program (2023YFB4404200), the Opening Project of Science and Technology on Reliability Physics and Application Technology of

Electronic Component Laboratory (ZHD202305), and the Foshan science and technology innovation project (2320001007250).

References

1 Y. Liu, J. Zhou, Z. Ning, H. Huang, Z. Cheng, L. Duan, Y. Wang, X. Tao, P. Liu, Y. Ma and Z. Yao, Multi-Interfacial Heterostructure Design of Carbon Fiber/Silicone Rubber-Oriented Composites for Microwave Absorption and Thermal Management, *Adv. Funct. Mater.*, 2024, **34**, 2411573.

2 H. Chen, Z. Huang, Y. Huang, Y. Zhang, Z. Ge, W. Ma, T. Zhang, M. Wu, S. Xu, F. Fan, S. Chang and Y. Chen, Consecutively Strong Absorption from Gigahertz to Terahertz Bands of a Monolithic Three-Dimensional Fe_3O_4/Graphene Material, *ACS Appl. Mater. Interfaces*, 2019, **11**, 1274–1282.

3 P. Liu, V. M. H. Ng, Z. Yao, J. Zhou, Y. Lei, Z. Yang, H. Lv and L. B. Kong, Facile Synthesis and Hierarchical Assembly of Flowerlike Nio Structures with Enhanced Dielectric and Microwave Absorption Properties, *ACS Appl. Mater. Interfaces*, 2017, **9**, 16404–16416.

4 J. Feng, Y. Zong, Y. Sun, Y. Zhang, X. Yang, G. Long, Y. Wang, X. Li and X. Zheng, Optimization of Porous $Feni_3$/N-Gn Composites with Superior Microwave Absorption Performance, *Chem. Eng. J.*, 2018, **345**, 441–451.

5 L. Duan, J. Zhou, Y. Yan, J. Tao, Y. Liu, Y. Lei, K. Zou, Y. Wang, H. Huang, X. Tao, P. Liu, Y. Ma and Z. Yao, Electron Migratory Polarization of Interfacial Electric Fields Facilitates Efficient Microwave Absorption, *Adv. Funct. Mater.*, 2025, **35**, 2416727.

6 Y. Sun, J. Zhang, Y. Zong, X. Deng, H. Zhao, J. Feng, M. He, X. Li, Y. Peng and X. Zheng, Crystalline–Amorphous Permalloy@Iron Oxide Core–Shell Nanoparticles Decorated on Graphene as High-Efficiency, Lightweight, and Hydrophobic Microwave Absorbents, *ACS Appl. Mater. Interfaces*, 2019, **11**, 6374–6383.

7 L. Su, M. Li, H. Wang, M. Niu, D. Lu and Z. Cai, Resilient Si_3n_4 Nanobelt Aerogel as Fire-Resistant and Electromagnetic Wave-Transparent Thermal Insulator, *ACS Appl. Mater. Interfaces*, 2019, **11**, 15795–15803.

8 B. Zhao, Z. Yan, Y. Du, L. Rao, G. Chen, Y. Wu, L. Yang, J. Zhang, L. Wu, D. W. Zhang and R. Che, High-Entropy Enhanced Microwave Attenuation in Titanate Perovskites, *Adv. Mater.*, 2023, **35**, 2210243.

9 L. Zhou, P. Hu, M. Bai, N. Leng, B. Cai, H.-L. Peng, P.-Y. Zhao, Y. Guo, M. He, G.-S. Wang and J. Gu, Harnessing the Electronic Spin States of Single Atoms for Precise Electromagnetic Modulation, *Adv. Mater.*, 2025, **37**, 2418321.

10 A. Sharbati, J. Mola Verdi Khani and G. R. Amiri, Microwave Absorption Studies of Nanocrystalline Prepared by the Citrate Sol–Gel Method, *Solid State Commun.*, 2012, **152**, 199–203.

11 S. Sutradhar, S. Das and P. K. Chakrabarti, Magnetic and Enhanced Microwave Absorption Properties of Nanoparticles of $Li_{0.32}Zn_{0.26}Cu_{0.1}Fe_{2.32}O_4$ Encapsulated in Carbon Nanotubes, *Mater. Lett.*, 2013, **95**, 145–148.

12 W. Wang, S. P. Gumfekar, Q. Jiao and B. Zhao, Ferrite-Grafted Polyaniline Nanofibers as Electromagnetic Shielding Materials, *J. Mater. Chem. C*, 2013, **1**, 2851–2859.

13 P. Liu, Z. Yao, J. Zhou, Z. Yang and L. B. Kong, Small Magnetic Co-Doped Nizn Ferrite/Graphene Nanocomposites and Their Dual-Region Microwave Absorption Performance, *J. Mater. Chem. C*, 2016, **4**, 9738–9749.

14 P. Xu and Z. Nan, Facile Synthesis of Magnetic Hollow Mesoporous Silica Spheres with Assembled Shell by Nanosheets as an Excellent Adsorbent, *Mater. Lett.*, 2018, **218**, 209–212.

15 H. Zhang, A. Xie, C. Wang, H. Wang, Y. Shen and X. Tian, Novel Rgo/A-Fe_2o_3 Composite Hydrogel: Synthesis, Characterization and High Performance of Electromagnetic Wave Absorption, *J. Mater. Chem. A*, 2013, **1**, 8547–8552.

16 Z. K. Huang, Y. T. Chen, L. G. Xu, J. P. Peng and P. J. Liu, Patterned Au@Ag Nanoparticles for Surface-Enhanced Raman Scattering, *ACS Appl. Nano Mater.*, 2024, **7**(21), 25099–25106.

17 F. Meng, H. Wang, F. Huang, Y. Guo, Z. Wang, D. Hui and Z. Zhou, Graphene-Based Microwave Absorbing Composites: A Review and Prospective, *Composites, Part B*, 2018, **137**, 260–277.

18 Z. Li, X. Li, Y. Zong, G. Tan, Y. Sun, Y. Lan, M. He, Z. Ren and X. Zheng, Solvothermal Synthesis of Nitrogen-Doped Graphene Decorated by Superparamagnetic Fe_3O_4 Nanoparticles and Their Applications as Enhanced Synergistic Microwave Absorbers, *Carbon*, 2017, **115**, 493–502.

19 K. Bogdan, D. André, W. C. Aron, R. P. Stephen, R. Stephan and P. D. Saroj, 1d Ferromagnetic Edge Contacts to 2d Graphene/H-Bn Heterostructures, *2D Mater.*, 2018, **5**, 014001.

20 H.-Y. Wang, P. Hu, X.-B. Sun, Z.-L. Hou, P.-Y. Zhao, L. Zhou, S.-H. Yang, C. Geng, Y. Zhu, X. Wu and G.-S. Wang, Bioinspired Disordered Aerogel for Omnidirectional Terahertz Response, *Adv. Mater.*, 2025, **37**, 2418889.

21 M. Han, X. Yin, K. Hantanasirisakul, X. Li, A. Iqbal, C. B. Hatter, B. Anasori, C. M. Koo, T. Torita, Y. Soda, L. Zhang, L. Cheng and Y. Gogotsi, Anisotropic Mxene Aerogels with a Mechanically Tunable Ratio of Electromagnetic Wave Reflection to Absorption, *Adv. Opt. Mater.*, 2019, **7**, 1900267.

22 F. Shahzad, M. Alhabeb, C. B. Hatter, B. Anasori, S. M. Hong, C. M. Koo and Y. Gogotsi, Electromagnetic Interference Shielding with 2d Transition Metal Carbides (Mxenes), *Science*, 2016, **353**, 1137–1140.

23 X. Li, X. Yin, C. Song, M. Han, H. Xu, W. Duan, L. Cheng and L. Zhang, Self-Assembly Core–Shell Graphene-Bridged Hollow Mxenes Spheres 3d Foam with Ultrahigh Specific Em Absorption Performance, *Adv. Funct. Mater.*, 2018, **28**, 1803938.

24 Y. Du, Z. Yan, W. You, Q. Men, G. Chen, X. Lv, Y. Wu, K. Luo, B. Zhao, J. Zhang and R. Che, Balancing Mxene Surface Termination and Interlayer Spacing Enables Superior Microwave Absorption, *Adv. Funct. Mater.*, 2023, **33**, 2301449.

25 R. Deng, B. Chen, H. Li, K. Zhang, T. Zhang, Y. Yu and L. Song, Mxene/Co_3o_4 Composite Material: Stable Synthesis and Its Enhanced Broadband Microwave Absorption, *Appl. Surf. Sci.*, 2019, **488**, 921–930.

26 M. K. Han, X. W. Yin, H. Wu, Z. X. Hou, C. Q. Song, X. L. Li, L. T. Zhang and L. F. Cheng, Ti_3c_2 Mxenes with Modified Surface for High-Performance Electromagnetic Absorption and Shielding in the X-Band, *ACS Appl. Mater. Interfaces*, 2016, **8**, 21011–21019.

27 M.-S. Cao, W.-L. Song, Z.-L. Hou, B. Wen and J. Yuan, The Effects of Temperature and Frequency on the Dielectric Properties, Electromagnetic Interference Shielding and Microwave-Absorption of Short Carbon Fiber/Silica Composites, *Carbon*, 2010, **48**, 788–796.

28 S. Ni, X. Sun, X. Wang, G. Zhou, F. Yang, J. Wang and D. He, Low Temperature Synthesis of Fe_3o_4 Micro-Spheres and Its Microwave Absorption Properties, *Mater. Chem. Phys.*, 2010, **124**, 353–358.

29 M. Fu, Q. Jiao and Y. Zhao, Preparation of $Nife_2O_4$ Nanorod-Graphene Composites Via an Ionic Liquid Assisted One-Step Hydrothermal Approach and Their Microwave Absorbing Properties, *J. Mater. Chem. A*, 2013, **1**, 5577–5586.

30 M. Naguib, O. Mashtalir, J. Carle, V. Presser, J. Lu, L. Hultman, Y. Gogotsi and M. W. Barsoum, Two-Dimensional Transition Metal Carbides, *ACS Nano*, 2012, **6**, 1322–1331.

31 M. R. Lukatskaya, O. Mashtalir, C. E. Ren, Y. Dall'Agnese, P. Rozier, P. L. Taberna, M. Naguib, P. Simon, M. W. Barsoum and Y. Gogotsi, Cation Intercalation and High Volumetric Capacitance of Two-Dimensional Titanium Carbide, *Science*, 2013, **341**, 1502–1505.

32 S. Kajiyama, L. Szabova, K. Sodeyama, H. Iinuma, R. Morita, K. Gotoh, Y. Tateyama, M. Okubo and A. Yamada, Sodium-Ion Intercalation Mechanism in Mxene Nanosheets, *ACS Nano*, 2016, **10**, 3334–3341.

33 Y. Qian, H. Wei, J. Dong, Y. Du, X. Fang, W. Zheng, Y. Sun and Z. Jiang, Fabrication of Urchin-Like Zno-Mxene Nanocomposites for High-Performance Electromagnetic Absorption, *Ceram. Int.*, 2017, **43**, 10757–10762.

34 C. Li, S. Yu, S. Luo, W. Yang, Z. Ge, H. Huang, R. Sun and C.-P. Wong, Enhancement of Dielectric Performance Upto Ghz of the Composites with Polymer Encapsulated Hybrid $Batio_3$–Cu as Fillers: Multiple Interfacial Polarizations Playing a Key Role, *RSC Adv.*, 2016, **6**, 36450–36458.

35 P. Liu, Z. Yao, V. M. H. Ng, J. Zhou, L. B. Kong and K. Yue, Facile Synthesis of Ultrasmall Fe_3o_4 Nanoparticles on Mxenes for High Microwave Absorption Performance, *Composites, Part A*, 2018, **115**, 371–382.

36 Y.-X. Bai, D.-P. Liu, L. Zhou, B. Cai, P.-Y. Zhao, H.-L. Peng, Y. Zhang, Q.-F. Xuan, W.-H. Liang, Z.-L. Hou and G.-S. Wang, High-Performance Wave Loss Capability by Constructing Well-Defined Hierarchical Aerogel Framework with Strongly Coupled Carbon/Ceo_2 Interface, *Chem. Eng. J.*, 2025, **504**, 158873.

37 P. Liu, Z. Yao and J. Zhou, Preparation of Reduced Graphene Oxide/$Ni_{0.4}Zn_{0.4}Co_{0.2}Fe_2O_4$ Nanocomposites and Their Excellent Microwave Absorption Properties, *Ceram. Int.*, 2015, **41**, 13409–13416.

38 D. Sarkar, A. Bhattacharya, P. Nandy and S. Das, Enhanced Broadband Microwave Reflection Loss of Carbon Nanotube Ensheathed Ni–Zn–Co-Ferrite Magnetic Nanoparticles, *Mater. Lett.*, 2014, **120**, 259–262.

39 S. Myhra, J. A. A. Crossley and M. W. Barsoum, Crystal-Chemistry of the Ti_3alc_2 and Ti_4aln_3 Layered Carbide/Nitride Phases—Characterization by Xps, *J. Phys. Chem. Solids*, 2001, **62**, 811–817.

40 C. Peng, X. Yang, Y. Li, H. Yu, H. Wang and F. Peng, Hybrids of Two-Dimensional Ti_3c_2 and Tio_2 Exposing {001} Facets toward Enhanced Photocatalytic Activity, *ACS Appl. Mater. Interfaces*, 2016, **8**, 6051–6060.

41 A. E. Berkowitz, W. J. Schuele and P. J. Flanders, Influence of Crystallite Size on the Magnetic Properties of Acicular Γ-Fe_2O_3 Particles, *J. Appl. Phys.*, 1968, **39**, 1261–1263.

42 P. Liu, Z. Yao, V. M. H. Ng, J. Zhou and L. B. Kong, Novel Multilayer-Like Structure of Ti_3c_2tx/Cnzf Composites for Low-Frequency Electromagnetic Absorption, *Mater. Lett.*, 2019, **248**, 214–217.

43 H. Wang, Y. Y. Dai, D. Y. Geng, S. Ma, D. Li, J. An, J. He, W. Liu and Z. D. Zhang, Coxni100-X Nanoparticles Encapsulated by Curved Graphite Layers: Controlled in Situ Metal-Catalytic Preparation and Broadband Microwave Absorption, *Nanoscale*, 2015, **7**, 17312–17319.

44 B. Zhao, W. Zhao, G. Shao, B. Fan and R. Zhang, Morphology-Control Synthesis of a Core–Shell Structured Nicu Alloy with Tunable Electromagnetic-Wave Absorption Capabilities, *ACS Appl. Mater. Interfaces*, 2015, **7**, 12951–12960.

45 S. L. Wen, Y. Liu, X. C. Zhao, J. W. Cheng and H. Li, Synthesis, Dual-Nonlinear Magnetic Resonance and Microwave Absorption Properties of Nanosheet Hierarchical Cobalt Particles, *Phys. Chem. Chem. Phys.*, 2014, **16**, 18333–18340.

46 X. Tian, F. Meng, F. Meng, X. Chen, Y. Guo, Y. Wang, W. Zhu and Z. Zhou, Synergistic Enhancement of Microwave Absorption Using Hybridized Polyaniline@Helical Cnts with Dual Chirality, *ACS Appl. Mater. Interfaces*, 2017, **9**, 15711–15718.

47 Y. Li, X. Zhou, J. Wang, Q. Deng, M. Li, S. Du, Y.-H. Han, J. Lee and Q. Huang, Facile Preparation of in Situ Coated $Ti_3c_2t_x$/$Ni_{0.5}Zn_{0.5}Fe_2O_4$ Composites and Their Electromagnetic Performance, *RSC Adv.*, 2017, **7**, 24698–24708.

48 P. Liu, Z. Yao and J. Zhou, Controllable Synthesis and Enhanced Microwave Absorption Properties of Silane-Modified $Ni_{0.4}Zn_{0.4}Co_{0.2}Fe_2O_4$ Nanocomposites Covered with Reduced Graphene Oxide, *RSC Adv.*, 2015, **5**, 93739–93748.

49 B. Kuang, W. Song, M. Ning, J. Li, Z. Zhao, D. Guo, M. Cao and H. Jin, Chemical Reduction Dependent Dielectric Properties and Dielectric Loss Mechanism of Reduced Graphene Oxide, *Carbon*, 2018, **127**, 209–217.

50 Y. Du, W. Liu, R. Qiang, Y. Wang, X. Han, J. Ma and P. Xu, Shell Thickness-Dependent Microwave Absorption of Core-

Shell Fe_3O_4@C Composites, *ACS Appl. Mater. Interfaces*, 2014, **6**, 12997–13006.

51 B. Zhao, Y. Du, H. Lv, Z. Yan, H. Jian, G. Chen, Y. Wu, B. Fan, J. Zhang, L. Wu, D. W. Zhang and R. Che, Liquid-Metal-Assisted Programmed Galvanic Engineering of Core–Shell Nanohybrids for Microwave Absorption, *Adv. Funct. Mater.*, 2023, **33**, 2302172.

52 B. Zhao, Z. Yan, L. Liu, Y. Zhang, L. Guan, X. Guo, R. Li, R. Che and R. Zhang, A Liquid-Metal-Assisted Competitive Galvanic Reaction Strategy toward Indium/Oxide Core–Shell Nanoparticles with Enhanced Microwave Absorption, *Adv. Funct. Mater.*, 2024, **34**, 2314008.

53 P. Liu, V. M. H. Ng, Z. Yao, J. Zhou, Y. Lei, Z. Yang and L. B. Kong, Microwave Absorption Properties of Double-Layer Absorbers Based on $Co_{0.2}Ni_{0.4}Zn_{0.4}Fe_2O_4$ Ferrite and Reduced Graphene Oxide Composites, *J. Alloys Compd.*, 2017, **701**, 841–849.

54 Y. Li, X. Liu, X. Nie, W. Yang, Y. Wang, R. Yu and J. Shui, Multifunctional Organic-Inorganic Hybrid Aerogel for Self-Cleaning, Heat-Insulating, and Highly Efficient Microwave Absorbing Material, *Adv. Funct. Mater.*, 2019, **29**, 1807624.

55 H. J. Wu, G. L. Wu, Y. Y. Ren, L. Yang, L. D. Wang and X. H. Li, Co^{2+}/Co^{3+} Ratio Dependence of Electromagnetic Wave Absorption in Hierarchical $Nico_2O_4$-$Conio_2$ Hybrids, *J. Mater. Chem. C*, 2015, **3**, 7677–7690.

56 P. Liu, S. Chen, M. Yao, Z. Yao, V. M. H. Ng, J. Zhou, Y. Lei, Z. Yang and L. B. Kong, Delamination Strategy to Achieve Ti_3c_2tx/Cnzf Composites with Tunable Electromagnetic Absorption, *Mater. Sci. Semicond. Process.*, 2020, **112**, 105008.

57 P.-J. Liu, Z.-J. Yao, V. M. H. Ng, J.-T. Zhou, Z.-H. Yang and L.-B. Kong, Enhanced Microwave Absorption Properties of Double-Layer Absorbers Based on Spherical Nio and $Co_{0.2}Ni_{0.4}Zn_{0.4}Fe_2O_4$ Ferrite Composites, *Acta Metall. Sin.*, 2018, **31**, 171–179.

58 X. H. Ren, H. Q. Fan and Y. K. Cheng, Microwave Absorption Properties of Double-Layer Absorber Based on Carbonyl Iron/Barium Hexaferrite Composites, *Appl. Phys. A:Mater. Sci. Process.*, 2016, **122**, 256–271.

59 B. Zhao, Y. Du, Z. Yan, L. Rao, G. Chen, M. Yuan, L. Yang, J. Zhang and R. Che, Structural Defects in Phase-Regulated High-Entropy Oxides toward Superior Microwave Absorption Properties, *Adv. Funct. Mater.*, 2023, **33**, 2209924.

60 H. Peng, B. Cai, Y. Zhang, L. Gao, P.-Y. Zhao, L. Zhou, S. Zhang, W. Liang, Q.-F. Xuan, M. C. Koo, C.-M. Liang, W.-P. Li, Z.-L. Hou, T. Zhou and G.-S. Wang, Radar-Terahertz-Infrared Compatible Stealth Coaxial Silver Nanowire@Carbon Nano-Cable Aerogel, *Angew. Chem.*, 2025, **137**, e202421090.

61 Z. Jiao, W. Huyan, F. Yang, J. Yao, R. Tan, P. Chen, X. Tao, Z. Yao, J. Zhou and P. Liu, Achieving Ultra-Wideband and Elevated Temperature Electromagnetic Wave Absorption Via Constructing Lightweight Porous Rigid Structure, *Nano-Micro Lett.*, 2022, **14**, 173.

62 J. Su, W. Zhou, Y. Liu, Y. Qing, F. Luo and D. Zhu, High-Temperature Dielectric and Microwave Absorption Property of Plasma Sprayed Ti_3sic_2/Cordierite Coatings, *J. Mater. Sci.: Mater. Electron.*, 2016, **27**, 2460–2466.

63 Q.-Q. Ni, G. J. H. Melvin and T. Natsuki, Double-Layer Electromagnetic Wave Absorber Based on Barium Titanate/Carbon Nanotube Nanocomposites, *Ceram. Int.*, 2015, **41**, 9885–9892.

64 Y. Zhao, L. Liu, J. Han, W. Wu and G. Tong, Effective Modulation of Electromagnetic Characteristics by Composition and Size in Expanded Graphite/Fe_3O_4 Nanoring Composites with High Snoek's Limit, *J. Alloys Compd.*, 2017, **728**, 100–111.

65 W. You, H. Bi, W. She, Y. Zhang and R. Che, Dipolar-Distribution Cavity Gamma-Fe_2O_3@C@Alpha-Mno_2 Nanospindle with Broadened Microwave Absorption Bandwidth by Chemically Etching, *Small*, 2017, **13**, 165620.

66 L. Zhang, N. Stalin, N. Tran, S. Mehrez, M. F. Badran, V. Mohanavel and Q. Xu, Development of High-Efficient Double-Layer Microwave Absorbers Based on 3d Cabbage-Like $Cofe_2O_4$ and Cauliflower-Like Polypyrrole, *Ceram. Int.*, 2022, **48**, 16374–16385.

67 H. Zhang, L. Gong, L. Yan, Y. Li, S. Tong, J. Xu, K. Zhang and J. Xiang, Design of Double-Layer Absorbers Based on Co_2y@C Core-Shell Nanofibers and Carbon Nanofibers for High-Efficient and Tunable Microwave Absorption, *J. Magn. Magn. Mater.*, 2023, **569**, 170394.

68 L. Li, X. Dang, R. Boudaghi and M. N. Akhtar, Microwave Absorption Characteristic of a Double-Layer X-Band Absorber Based on Mwcnts/$La_{0.6}Sr_{0.4}Mn_{0.5}Fe_{0.5}O_4$ Coated with Pedot Polymer, *Ceram. Int.*, 2021, **47**, 17736–17744.

69 Y. Li, X. Wu, J. Chen, A. Cao, R. Boudaghi and M. N. Akhtar, Effect of Filler Loading and Thickness Parameters on the Microwave Absorption Characteristic of Double-Layered Absorber Based on Mwcnt/$Batio_3$/Pitted Carbonyl Iron Composite, *Ceram. Int.*, 2021, **47**, 19538–19545.

70 X. Ye, C. Yang, E. He, P. Yang, Q. Gao, T. Yan, S. Yin, Y. Ye and H. Wu, Electromagnetic Wave Absorption Properties of the Fesial/Pla and Fesial-Mos_2-Graphene/Pla Double-Layer Absorber Formed by Fused Deposition Modeling, *J. Magn. Magn. Mater.*, 2023, **565**, 170280.

71 O. Mirzaee, I. Huynen and M. Zareinejad, Electromagnetic Wave Absorption Characteristics of Single and Double Layer Absorbers Based on Trimetallic Feconi@C Metal–Organic Framework Incorporated with Mwcnts, *Synth. Met.*, 2021, **271**, 116634.

72 Y. Ning, S. Yang, X. Sun, S. Wang, L. Liang, Y. Cheng, Y. Yuan and Y. Li, Enhanced Electromagnetic Absorption Properties of the Double-Layer Ti_3c_2tx Mxene Absorber with Orthogonal Microstructures, *J. Mater. Chem. C*, 2024, **12**, 6086–6097.

